Contents lists available at ScienceDirect

European Journal of Radiology

USPIO-enhanced MRI of lymph nodes in rectal cancer: A node-to-node comparison with histopathology

Rutger C.H. Stijns [a,b,*], Bart W.J. Philips [a], Iris D. Nagtegaal [c], Fatih Polat [d], Johannes H. W. de Wilt [b], Carla A.P. Wauters [e], Patrik Zamecnik [a], Jurgen J. Fütterer [a], Tom W.J. Scheenen [a,f]

[a] *Department of Radiology and Nuclear Medicine, Radboud University Medical Center, Nijmegen, the Netherlands*
[b] *Department of Surgery, Radboud University Medical Center, Nijmegen, the Netherlands*
[c] *Department of Pathology, Radboud University Medical Center, Nijmegen, the Netherlands*
[d] *Department of Surgery, Canisius-Wilhelmina Hospital, Nijmegen, the Netherlands*
[e] *Department of Pathology, Canisius-Wilhelmina Hospital, Nijmegen, the Netherlands*
[f] *Erwin L. Hahn Institute for MR Imaging, University of Duisburg-Essen, Essen, 45141, Germany*

ARTICLE INFO

ABSTRACT

Purpose: To evaluate the initial results of predicting lymph node metastasis in rectal cancer patients detected *in-vivo* with USPIO-enhanced MRI at 3 T compared on a node-to-node basis with histopathology.
Methods: Ten rectal cancer patients of all clinical stages were prospectively included for an *in-vivo* 0.85 mm^3 isotropic 3D MRI after infusion of Ferumoxtran-10. The surgical specimens were examined *ex-vivo* with an 0.29 mm^3 isotropic MRI examination. Two radiologists evaluated *in-vivo* MR images with a classification scheme to predict lymph node status. *Ex-vivo* MRI was used for MR-guided pathology and served as a key link between *in-vivo* MRI and final histopathology for the node-to-node analysis.
Results: 138 lymph nodes were detected by reader 1 and 255 by reader 2 ($p = 0.005$) on *in-vivo* MRI with a median size of 2.6 and 2.4 mm, respectively. Lymph nodes were classified with substantial inter-reader agreement ($\kappa = 0.73$). Node-to-node comparison was possible for 55 lymph nodes (median size 3.2 mm; range 1.2–12.3), of which 6 were metastatic on pathology. Low true-positive rates (3/26, 11 % for both readers) and high true negative rates were achieved (14/17, 82 %; 19/22, 86 %). Pathological re-evaluations of 20 lymph nodes with high signal intensity on USPIO-enhanced MRI without lymph node metastases (false positives) did not reveal tumor metastasis but showed benign lymph node tissue with reactive follicles.
Conclusions: High resolution MRI visualizes a large number of mesorectal lymph nodes. USPIO-enhanced MRI was not accurate for characterizing small benign versus small tumoral lymph nodes in rectal cancer patients. Suspicious nodes on *in-vivo* MRI occur as inflammatory as well as metastatic nodes.

1. Introduction

The presence of lymph node metastases in rectal cancer is a key factor in determining prognosis and treatment [1]. Diagnostic lymph node staging, however, is still a major challenge [2–4]. Over the past decade multiple imaging approaches have been assessed as a biomarker to differentiate between benign and malignant lymph nodes [5–10]. The size and shape of a lymph node as sole criteria are unreliable measures to predict lymph status, since metastatic lymph nodes in rectal cancer are often smaller than 5 mm [11,12]. Moreover, variation in interpreting MR images leads to predominantly upstaging with potential effects on treatment [4,13]. Therefore, there is a need for a more accurate prediction of the presence of lymph node metastases.

Ferumoxtran-10, consisting of ultrasmall superparamagnetic iron oxide (USPIO) particles that become lymphotropic after intravenous administration, has previously proven to be a valuable MRI-contrast

agent for detecting lymph node metastases [14–16]. Promising clinical results for USPIO-enhanced MRI were shown with a pooled sensitivity of 90 % and specificity of 96 % for multiple solid tumors [17]. USPIO-enhanced MRI also showed reproducible results in differentiating lymph node metastases in rectal cancer patients [18–20]. These studies were performed in clinical trials during the phase of clinical development of the product. However, high accuracy was described by detecting relatively large lymph nodes which have a higher probability of harboring metastases. Moreover, most studies were performed on 1.5 T MR systems with 2-dimensional (2D) multi-slice acquisitions, with known restrictions in resolution. It was demonstrated that especially the diagnostic accuracy for the detection of small lymph node metastases (<5 mm) dropped substantially [21]. By using 3-dimensional (3D) USPIO-enhanced MRI on a 3 T MR system, it is possible to increase the spatial resolution to small isotropic voxels, thereby potentially increasing the sensitivity for the detection of small (<5 mm) suspicious lymph nodes [22]. Identifying small lymph nodes that are suspicious for tumor metastases prior to surgery will contribute in planning for adequate treatment. However, whether the smallest lymph nodes that retain MR signal intensity after administration of USPIO nanoparticles indeed contain metastases requires a meticulous node-to-node validation. To provide more insight in the potential accuracy of predicting small lymph node metastases by using 3D USPIO-enhanced MRI, *in-vivo* detected suspicious lymph nodes have to be evaluated up to final histopathological analysis of the identical nodes after resection.

Therefore, in this study, we aim to present the initial results of the histopathological node-to-node validation of lymph nodes that are detected *in-vivo* with sub-mm resolution on 3D USPIO-enhanced MRI at 3 T in rectal cancer patients.

2. Material and methods

The authors had full control of the data and information submitted for publication. The study was approved by the institutional review boards of the two participating hospitals (NL51335.091.14 & NL58295.091.16) and written informed consents were obtained from all patients. The study was registered in clinicaltrials.gov (NCT02751606). Ferumoxtran-10 (SPL Medical B.V., Nijmegen, The Netherlands) is an USPIO contrast agent currently undergoing a multicenter registration study in Germany, Switzerland and the Netherlands. The contrast agent is currently not commercially available.

2.1. Patient selection

In a prospective, two center, diagnostic cohort study in the period March 2017 to January 2018 patients from two referral centers with biopsy-proven rectal cancer were included. According to clinical endoscopic findings, rectal tumors were located within 15 cm from the anorectal junction. All patients had to undergo a surgical resection according to the principle of a total mesorectal excision (TME) [23]. In case of locally advanced rectal cancer (LARC; cT3-,MRF + or cT4), neoadjuvant chemoradiotherapy (nCRT) was admitted with an increased interval to surgery [24]. nCRT consisted of 25 fractions of 2 Gray combined with capecitabine 825 mg/m^2. Five patients underwent neoadjuvant treatment. Lymph nodes of (non)irradiated patients were compared for radiological and histological differences. The workflow of the study and number of patients asked for inclusion are shown in a STARD flow-diagram (Supplemental Fig. 1). Exclusion criteria were previous allergic reaction to contrast agents, contra-indication for MR investigation and the presence of a malignancy other than rectal cancer.

2.2. USPIO agent infusion and USPIO-enhanced MRI

The *in-vivo* USPIO-enhanced MRI was performed within 2 weeks prior to surgery. 24−36 h prior to the examination, patients were slowly intravenously infused with the USPIO particles (Ferumoxtran-10,

2.6 mg/kg body weight diluted in saline). MR imaging was performed at 3 T (Siemens Magnetom® Prisma, Erlangen, Germany) using a spine coil and a phased array body coil. Patients were supine, feet first positioned and received antispasmodic medication intramuscularly (1 mL Scopolamine Butyl Bromide, Sanofi-aventis Netherlands B.V.) unless a contraindication was present. The MR-protocol consisted of a 3D T1-weighted volume-interpolated gradient echo sequence (VIBE-DIXON) for anatomical imaging and a 3D T2*-weighted multi-gradient echo (mGRE) sequence for recognition of uptake of the contrast agent in the lymph nodes. From the VIBE-DIXON sequence 4 image sets were generated: in-phase, opposed-phase, water-only and fat-only. The in-phase images were used for in vivo lymph node selection. Multiple mGRE images were condensed into one T2*-weighted computed echo time (TE = 12 msec) image for interpretation of the USPIO presence within the identified lymph nodes [25]. No non-enhanced MRI examinations were performed. Details of the specific pulse sequences are shown in Table 1.

2.3. Evaluation of the USPIO-enhanced in-vivo MRI scans

In-vivo images were evaluated separately by two experienced abdominal radiologists (JF/R1 10 and PZ/R2 15 years, respectively), of whom one had experience with USPIO-enhanced MRI. The readers were blinded to clinical data, histology and each other's findings. All discovered lymph nodes and their locations were annotated in different datasets for both readers. Information regarding a lymph node that could be selected by one reader and not by the other, was not shared. Only mesorectal lymph nodes were selected on T1-weighted MR images and annotated by both readers, since these nodes could be compared with the *ex-vivo* MRI. Annotation of the detected lymph nodes was done using an annotation tool of the software package MeVisLab (MeVis Medical Solutions, Fraunhofer MEVIS). Short axis size of the lymph nodes was measured in the transverse plane of the "in phase" T1-weighted MR images. The appearances of lymph nodes on T2*-weighted MR images were classified for suspicion on containing metastases using a modified classification scheme based on nodal signal intensity and architecture (Table 2) [26]. In case of discrepancies between the classification of the readers (high signal intensity type 1–2 versus attenuated signal intensity type 6–7), they were asked to re-evaluate that lymph node resulting in a consensus read.

2.4. Ex-vivo MRI of the surgical specimen of the rectum

After surgery, all TME specimens were fixated in 10 % buffered formalin for at least 24 h. MR imaging of the fixated specimens was

Table 1

Imaging parameters of the 3 and 7 T MRI scan protocol. From the DIXON VIBE sequence 4 image sets were generated: in-phase, opposed-phase, water-only and fat-only. The in-phase images were used for in vivo lymph node selection.

3 T MRI protocol		
	T1 DIXON VIBE	3D Multi GRE
Plane	3D	3D
Repetition time (msec)	5.8	21.0
Echo time (msec)	1.2, 2.5	3.6 - 17.2
Matrix	384*384*192	384*384*224
Flip angle	10	10
resolution (mm^3)	$0.85 \times 0.85 \times 0.85$	$0.85 \times 0.85 \times 0.85$

7 T ex vivo MRI protocol		
	Lipid excitation GRE	Water excitation GRE
Plane	3D	3D
Repetition time (msec)	15.0	30
Echo time (msec)	3.0	6.2
Matrix	320*320*256	320*320*256
Flip angle	10	14
resolution (mm^3)	$0.29 \times 0.29 \times 0.29$	$0.29 \times 0.29 \times 0.29$

Table 2
Nodal types based on their characteristics on USPIO-enhanced MRI, derived from the classification scheme published by Harisinghani et al.(25).

Nodal type	Post Dose	Description
1		No blackening of node or node is hyperintense to surrounding tissue; heterogeneous or homogeneous achitecture
2		Node has central high signal with darkening along the peripheral rim; heterogeneous architecture
3		Partial darkening whereby more than 50 % of the node has area of high signal intensity; heterogeneous architecture
4		Less than 50 % of node has high signal intensity; heterogeneous architecture
5		Node having an overall dark signal other than central or hilar area of fat seen on T1 sequence
6		Node having an overall dark signal with speckles of subtles granulairities, homogeneous architecture
7		Node having an overall dark signal intensity; homogeneous architecture

performed on a horizontal 7 T preclinical MR system (ClinScan, Bruker® BioSpin, Ettlingen, Germany). The *ex vivo* MRI examinations were performed 1–2 weeks after Ferumoxtran-10 infusion, thus were not USPIO-enhanced. *Ex-vivo* images were evaluated by the coordinating physician (not one of the radiologists) by annotating lymph nodes located in the mesorectum detected on lipid and water selective GRE images [27]. Lymph nodes were defined as such in case of a spherical structure visible in three dimensions with low signal intensity on lipid and high signal intensity on water selective GRE images. When in doubt whether a structure could be a lymph node, it was not annotated. Sizes of the lymph nodes were measured in the transverse plane on water selective GRE images. Surgical specimens were further processed after lymph node recognition was completed. The *ex-vivo* images of the specimens were used as a key link between *in-vivo* MRI and histopathology.

2.5. Pathological evaluation

Pathological evaluation was performed by two experienced colorectal cancer pathologists (IN 22 and CW 25 years, respectively), one at each including center, according to the method described by Quirke et al. [28]. During macroscopical evaluation, TME specimens were sliced into 5 mm thick transverse tissue lamina. Each transverse tissue slice was evaluated for harboring lymph nodes. The coordinating physician together with one of the pathologists used ex-vivo MR data of the TME specimen during macroscopical examination as a guidance for lymph node harvesting [27]. Whenever a lymph node could not be detected in the specimen, but was likely a lymph node on ex-vivo MRI, samples of fatty tissue of that section were separately enclosed. Additionally, immunohistochemical CD68 staining could be performed to objectify the presence of macrophages that are responsible for macrophage-linked accumulation of USPIO particles [29].

2.6. Node-to-node analysis

All lymph nodes were annotated on *in-vivo* MRI, *ex-vivo* MRI and the corresponding tissue cassettes. Node-to-node matching was achieved by manually matching nodes from *in-vivo* MRI to *ex-vivo* MRI, and subsequently from *ex-vivo* MRI to pathology of the corresponding cassette. Lymph nodes visible on *in-vivo* MRI, but could not be matched to *ex-vivo* MRI were not included analysis. This also held for lymph nodes detected during pathology, but could not be matched to a lymph node on *ex-vivo* MRI. From this node-to-node analysis and a binary distinction in *in-vivo*

MRI nodal scores (type 1–2-3 is positive, type 4−5-6−7 is negative) true/false positives and negatives could be extracted with histopathology as ground truth.

2.7. Statistical analysis

The goal of the study was to compare *in-vivo* detected lymph nodes on USPIO-enhanced MRI with histopathology on a node-to-node basis. Numbers, largest diameter and percentages of detected lymph nodes were measured from all three modalities. Numbers and sizes were displayed in histograms (GraphPad Software, Inc). The results of the USPIO-enhanced MRI interpretations for both readers were assessed in cross tabulations. Inter-reader variability for all *in-vivo* scored lymph nodes was calculated using nodal types documented and by using a dichotomous parameter of the nodal types, dividing lymph nodes in two cohorts with (1) predominantly high-signal regions (type 1–2-3, no iron uptake) and (2) predominantly attenuated signal regions (type 4−5-6−7, iron uptake). Lymph nodes detected by only one of the radiologists were discarded for the inter-reader variability. The agreement of the nodal typing of the lymph nodes by the readers was measured by calculating the Cohen's Kappa (κ) value (poor if $\kappa \leq 0.20$, fair if $0.21 \leq \kappa \leq 0.40$, moderate if $0.41 \leq \kappa \leq 0.60$, substantial if $0.61 \leq \kappa \leq 0.80$, good if $\kappa > 0.80$).

Only lymph nodes that could be matched from *in-vivo* to histopathology were used in the validation analysis, of which the endpoint was the diagnostic performance of the USPIO-enhanced MRI. T-tests, χ^2 tests and Mann Whitney-U tests were used to determine the statistical significance of differences for ordinal and categorical variables (IBM SPSS Statistics, version 22). A p value of less than 0.05 was considered as statistically significant.

3. Results

Ten patients were included, of whom 2 female and 8 male patients with a mean age of 64 years (SD 7.7). 5 patients were scheduled for TME surgery only (staged 4 cT2N0, 1 cT3N0) and 5 patients for nCRT followed by TME (staged: 1 cT3N1, MRF+, 2 cT3N2 and 2 cT4N2). Surgery consisted of a low anterior resection (5) or abdominoperineal resection (5). Pathology revealed moderate to well differentiated adenocarcinomas in all patients. The TME specimens were of a mean size of 21.4 cm (SD 4.0). Ten complete *in-vivo* and *ex-vivo* datasets were retrieved. An example of *in-vivo* MRI is given in Fig. 1. No allergic reactions to the infusion of ferumoxtran-10 were observed.

R1 detected a total of 138 lymph nodes with a median size of 2.6 mm (range 1.2–12.3). R2 detected 255 lymph nodes with a median size of 2.4 mm (range 0.9–12.3). Per patient, this was a median number of 13 (7–24) lymph nodes for R1 and 23 (15–54) lymph nodes for R2. The total number of detected lymph nodes per patient differed between the two readers ($p = 0.005$). No peritumoral deposits were described. All nodal enhancement types were described of which type 1 (23.9 % and 18.8 %, reader 1 and 2) and type 7 (55.8 % and 43.1 %; R1,R2) most frequently. An overview of all classified nodes is shown in Table 3. Sixteen lymph nodes were scored with large discrepancies by the readers and were rescored as a type 1 (N = 7) and as a type 7 (N = 9). Nodal classification for the nodes detected by the two observers was performed with moderate agreement (κ = 0.433), which improved to a substantial agreement with the subdivision nodal type 1–2-3 versus 4−5-6−7 (κ = 0.732).

On *ex-vivo* images, 428 lymph nodes within the 10 specimens were annotated with a median size of 2.1 mm (range 0.7–8.9). During pathological examination, 216 lymph nodes, of which 19 metastatic, were discovered with a median size of 2.9 mm (range 0.7–16.9). This means that *ex-vivo* MRI revealed more lymph nodes than that could be discovered during pathological examination. One specimen was macroscopically evaluated without *ex-vivo* MR guidance. Size distribution of all lymph nodes separately detected on all three modalities are
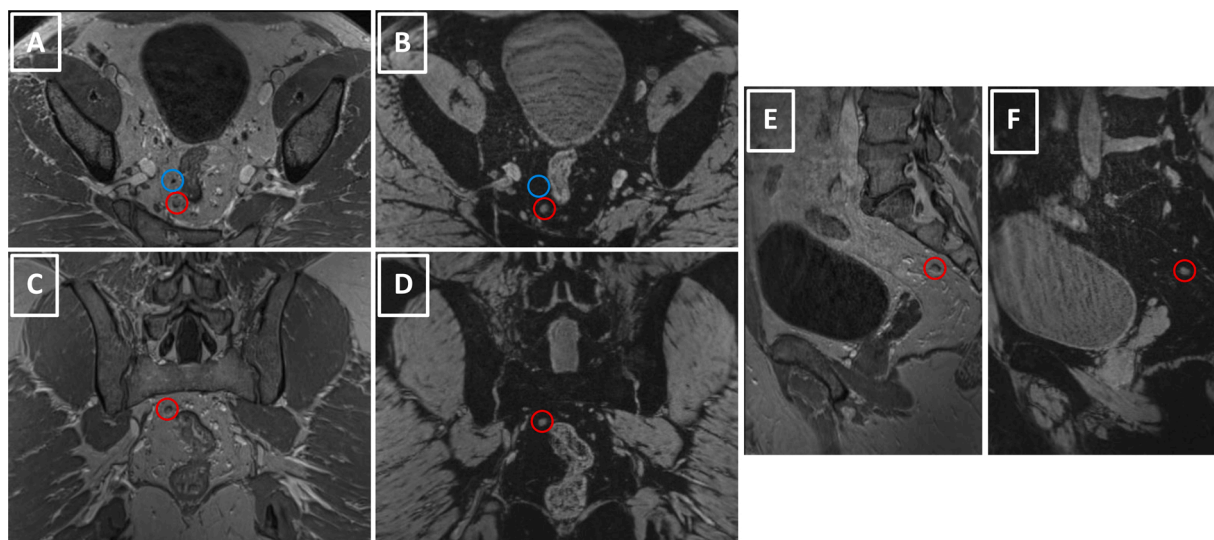
Fig. 1. Example of two lymph nodes detected on the *in-vivo* 3D T1-weighted DIXON-VIBE images and the 3D T2*-weighted mGRE images 24-36 h after infusion of Ferumoxtran-10. Both image sets are displayed in three orientations: a transverse view on A (T1-weighted) and B (T2*-weighted), a coronal view on C (T1-weighted) and D (T2*-weighted), and a sagittal view on E (T1-weighted) and F (T2*-weighted). The lymph node encircled in red on all displayed images (A-F) was rated as a type 1, 'high signal intensity' node. The lymph node encircled in blue on the axial images (A-B) was rated as a type 7, 'low signal intensity' node.

Table 3
Overview of different nodal types that were scored by the two readers appointed to the lymph nodes detected that were detected on *in-vivo* 3D MRI datasets.

	Nodal type described by reader 1 Frequency (%)	Nodal type described by reader 2 Frequency (%)
Type 1	33 (24 %)	48 (19 %)
Type 2	2 (1,5%)	39 (15 %)
Type 3	14 (10 %)	6 (3%)
Type 4	10 (7%)	18 (7%)
Type 5	0 (0%)	1 (1%)
Type 6	2 (1,5%)	31 (12 %)
Type 7	77 (56 %)	112 (43 %)
Total	138 (100 %)	255 (100 %)

displayed in Fig. 2A–D.

After comparing *in-vivo* with *ex-vivo* MR datasets, a node-to-node match from *in-vivo* to *ex-vivo* was possible for 70 lymph nodes. An example of correlating a lymph node from *in-vivo* MRI to *ex-vivo* MRI to final histopathology is given in Fig. 3. MR-guided pathology enabled a correlation from *ex-vivo* MRI to histopathology for 88 of the 216 lymph nodes. By combining these matching results, a match from *in-vivo* MRI to final histopathology was possible for a total of 55 lymph nodes, of which 43 (out of 138) lymph nodes scored by R1 and 49 (out of 255) lymph nodes scored by R2, respectively. The median size of the lymph nodes with a complete node-to-node match was 3.2 mm (range 1.2–12.3; size distribution displayed in Fig. 2E).

High signal intensity versus predominantly attenuated signal intensity regions was used for a comparison between USPIO-enhanced MRI appearance and pathologic diagnosis. For R1 and R2 respectively, the following rates were calculated: true positive rate of 11 % and 11 %; false positive rate of 89 % and 90 %; true negative rate of 82 % and 86 %; false negative rate 18 % and 14 % (Table 4). Sub-analysis comparing irradiated versus nonirradiated lymph nodes and lymph nodes harvested from low anterior versus abdominoperineal resection revealed no differences in false positive rates. Lymph nodes with predominantly high

signal intensity appeared as lymph node metastases on pathology in a minority of the cases (example shown in Fig. 4). Lymph nodes with attenuated signal on USPIO-enhanced MRI appeared frequently as normal lymph nodes (Fig. 5).

Twenty lymph nodes with high signal intensity on USPIO-enhanced MRI without lymph node metastases on initial histological evaluation were analyzed in further detail. Histological slides were reviewed for potentially missed tumor cells. Multiple new histological subsections were taken to detect metastasis throughout all compartments of the lymph nodes. These re-evaluations did not reveal tumor metastasis but showed benign lymph node tissue with reactive follicles. Additional staining immunohistochemistry with CD68 showed a normal distribution of macrophages throughout 6 selected lymph nodes (an example shown in Fig. 6). Iron deposits could also not be discovered during histopathological evaluation.

4. Discussion

The current study showed the first results of 3D USPIO-enhanced MRI on a 3 T MR-system. It was technically feasible to perform high-quality MR images of the mesorectum showing many detectable lymph nodes from 1 mm and larger in size. High-resolution 3D MRI enhanced with USPIO nanoparticles allowed the detection of small lymph nodes *in-vivo*, which required a renewed validation. The workflow with an intermediate *ex-vivo* MRI scan of a surgical specimen enabled a node-to-node validation in only 31 % and 19 % of the lymph nodes detected by two independent readers. Variations were seen in the number of detected lymph nodes on both *in-* and *ex-vivo* MRI and on histopathology. With *ex-vivo* MR imaging as a reference, 16.3 % of the lymph nodes could be related to *in-vivo* MRI and 20.6 % to definite histopathology, respectively.

Since the introduction of the USPIO nanoparticles, studies have shown high accuracy for malignant lymph node detection [30]. These results could not be reproduced. Where high signal intensity regions on iron-sensitive MRI were previously reported as highly predictive for tumor metastasis [19], suspicious lymph nodes in our cohort retained high MR signal intensity without a pathological substrate. Metastatic changes were seen on pathology in only a 6 of our evaluated suspicious lymph nodes (type 1–2-3). Apart from 3 lymph nodes that consisted predominantly of acellular mucin, most lymph nodes had a preserved, non-metastatic architecture with reactive lymph nodal follicles and
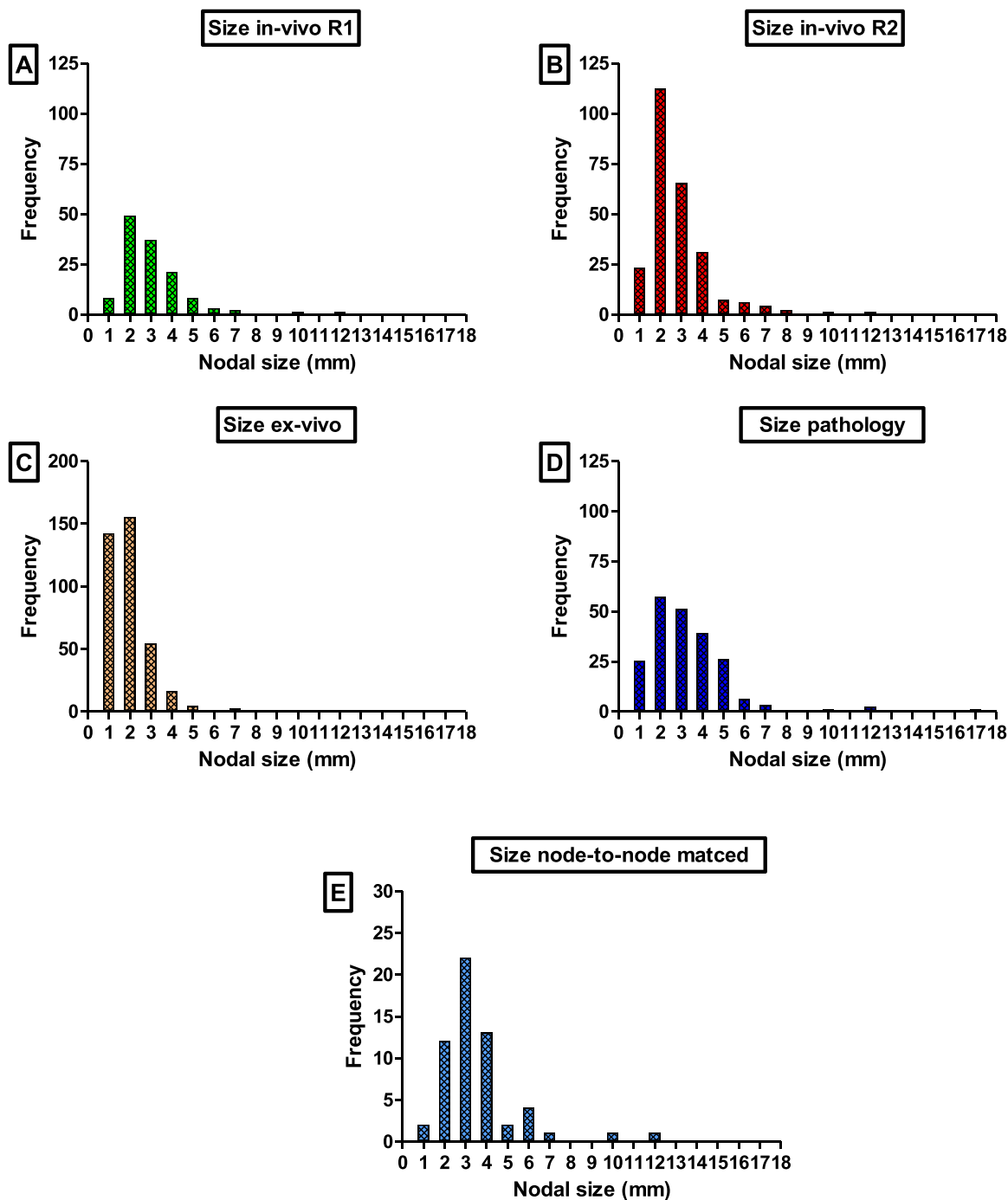
Fig. 2. Size distribution of all detected lymph nodes for the different detection methods. (A) shows the size distribution of the nodes detected by reader 1 on the *in-vivo* MRI dataset; (B) shows the size distribution of the nodes detected by reader 2 on the *in-vivo* MRI dataset; (C) shows the size distribution of the nodes detected on *ex-vivo* MRI dataset by the trained physician; (D) shows the size distribution of the nodes detected on histopathology; (E) shows the size distribution of the lymph nodes that were detected on all modalities and were matched on a node-to-node basis. The nodal size in (E) was measured at histopathology on the microscopical tissue slices.

macrophages present within the lymph nodes.

The high signal intensity in non-metastatic lymph nodes indicates a lack of USPIO-loaded macrophages or insufficient accumulation of iron particles in lymph nodes to cause a drop in signal intensity. This may be explained by an inflammatory response within these lymph nodes, either caused by the presence of the tumor, or as a consequence of nCRT. Although sub-analysis comparing irradiated versus nonirradiated lymph nodes revealed no differences, this observation might be due to the number of included patients. It is conceivable that an increased immune response with reactive lymphoid follicles could mimic a higher density

of cells and limit the accumulation of iron particles. Two studies reporting on USPIO appearance in inflammatory lymph nodes described both signal reduction as well as reduced USPIO particles in macrophages [20,31]. A reduced uptake of USPIO particles in macrophages could have led to higher signal intensities within nonmetastatic, inflammatory lymph nodes, but this was not investigated in further detail. Histological investigation in all dimensions of a subset of lymph nodes could not reveal small tumor deposits within the node which could have been an explanation for the remaining high signal intensity. The exact cause is of these high signal intensity lymph nodes on USPIO-enhanced MRI
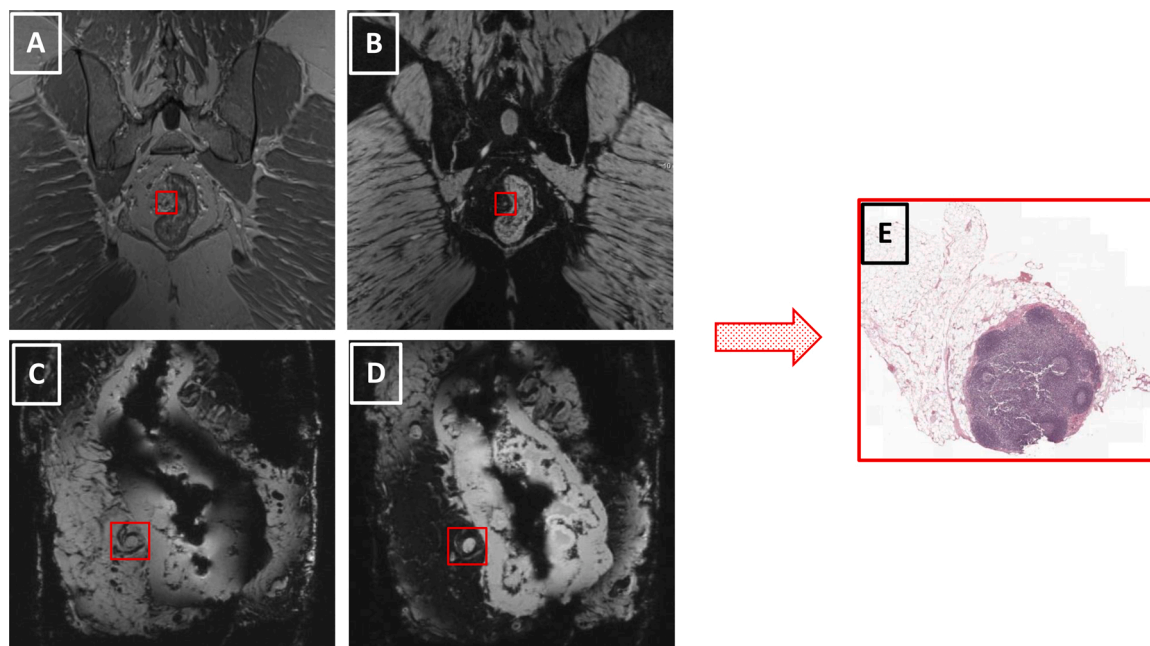
Fig. 3. Example of a lymph node that was seen on all three modalities, matched from *in-vivo* to *ex-vivo* MRI to histopathology. A and B show coronal views of one partition of 3D *in-vivo* MRI datasets 24-36 h after infusion of Ferumoxtran-10, of which A is the in-phase image of the VIBE-DIXON dataset and B is the T2*-weighted, iron-sensitive image of water content showing a type 1 lymph node. C and D show coronal views of lipid (C) and water (D) excited *ex-vivo* MRI. That same lymph node in the red box was identified in the specimen based on relative position with the rectum, blood vessels and other lymph nodes. E shows definite histopathology of the indicated lymph node of a size of 2.9 mm: normal follicular architecture without the presence of tumor metastasis.

Table 4
Cross tabulation of the definite pathological diagnosis compared to the lymph nodes with predominately high signal intensity (1,2,3) and attenuated signal intensity (4,5,6,7).

Reader 1	Pathology: metastasis	Pathology: no metastasis	Total	Reader 2	Pathology: metastasis	Pathology: no metastasis	Total
MR classification type 1,2,3	3	23	26	**MR classification type 1,2,3**	3	24	27
MR classification type 4,5,6,7	3	14	17	**MR classification type 4,5,6,7**	3	19	22
Total	6	37	43	**Total**	6	43	49

without tumor metastasis found on histology remains unclear.

The standardized classification scheme was used with substantial interobserver agreement between the two readers. Mainly lymph nodes with either high signal intensity or without signal were described, meaning that intermediate nodal appearances were not frequently seen. A large discrepancy was seen between the number of lymph nodes detected. Differences in numbers of detected mesorectal lymph nodes may be reader-dependent based on the experience of the radiologist or on the time that was invested in lymph node evaluation [32]. The evaluation time for each of the two MRI readers was not measured, but the time spent could partly account for the difference. Another reason could be the relative inexperience with the MRI sequences used for imaging lymph nodes located in the mesorectum. Although the number of detected lymph nodes differed, the classification of the nodes by both readers was very similar.

A final node-to-node match was not possible for many nodes detected by the readers. Challenges were found in both translations from *in-vivo* to *ex-vivo* MRI as well as from *ex-vivo* MRI to pathology. Firstly, due to differences in spatial resolution, not all nodes discovered on *ex-vivo* MRI could be discovered *in-vivo*. Secondly, lymph nodes scored *in-vivo* were located throughout the whole mesorectum and distal mesocolon and part of those could have remained in situ after surgery. Thirdly, formalin fixation could have interfered with the translation from *in-vivo* to *ex-vivo* MR, since it can lead to shrinkage and may alter anatomical references

compared to the *in-vivo* situation [33,34]. Fourthly, the challenging part in linking *ex-vivo* MRI to pathological examination was the translation from 3D to a 2D pathological work-up [27].

Previous studies of similar node-to-node comparisons of lymph nodes showed better outcomes without using an intermediate MRI scan [18,19]. However, spatial resolution of the 1.5 T MRI images was lower, and the number of detected lymph nodes per patient was much lower (333 nodes in pathology of 28 patients [19], versus 216 nodes in 10 patients in our study), indicating a bias towards larger nodes. With that study design, 62–65 % of the lymph nodes could be matched with a mean size diameter of 4.6–4.7 mm compared to our median 2.4–2.6 mm. In line with other studies, larger lymph nodes could also be more successfully linked to pathology. New imaging techniques with concomitant higher spatial resolution will visualize smaller structures, which will lead to challenges in translating imaging findings to the reference standard. Therefore, the size of lymph nodes plays a substantial role in the success of node-to-node matching.

A few limitations should be discussed. First, the translation from *in-vivo* to pathology had remaining challenges as described above, which led to a selection bias for larger lymph nodes included in the node-to-node analysis. Second, the size of the study cohort ideally would have been larger with a greater harvest of lymph nodes on imaging as well as on pathology. Despite the small number of included patients, a large number of lymph nodes could still be examined. Third, our study
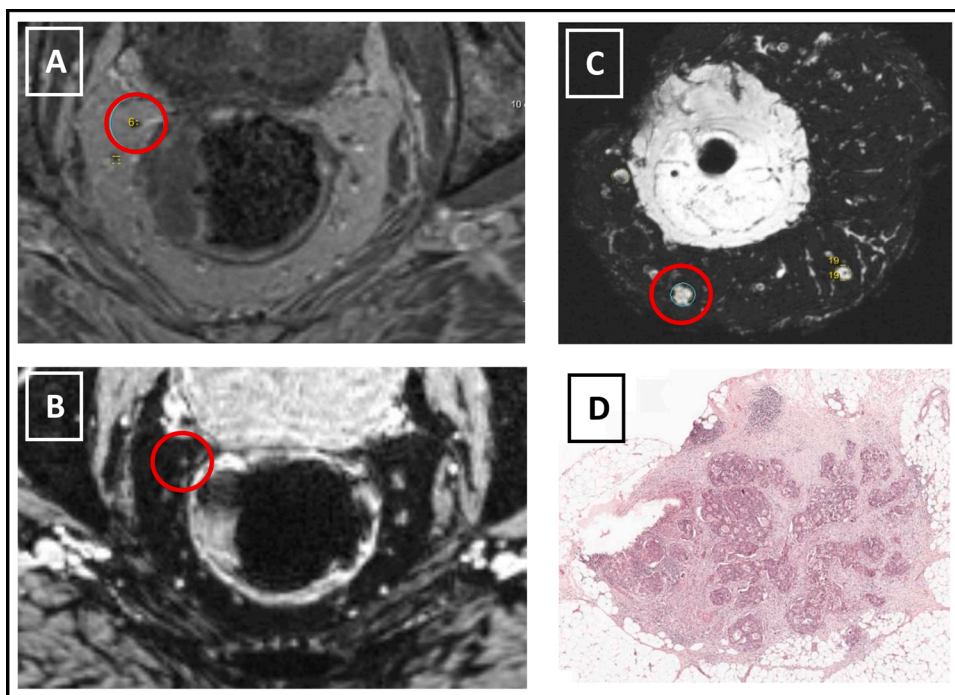
Fig. 4. Node-to-node matching of a metastatic lymph node (red circle). A lymph node displayed in the transverse plane of the in-phase image of the *in-vivo* VIBE-DIXON dataset (A), defined as nodal type 1 by both readers on the T2*-weighted, iron-sensitive image of water content (B) 24-36 h after infusion of Ferumoxtran-10. The node could be matched to the water selective *ex-vivo* MRI (C), which appeared to be a metastatic lymph node on histopathology (D). The primary tumor was staged cT3.
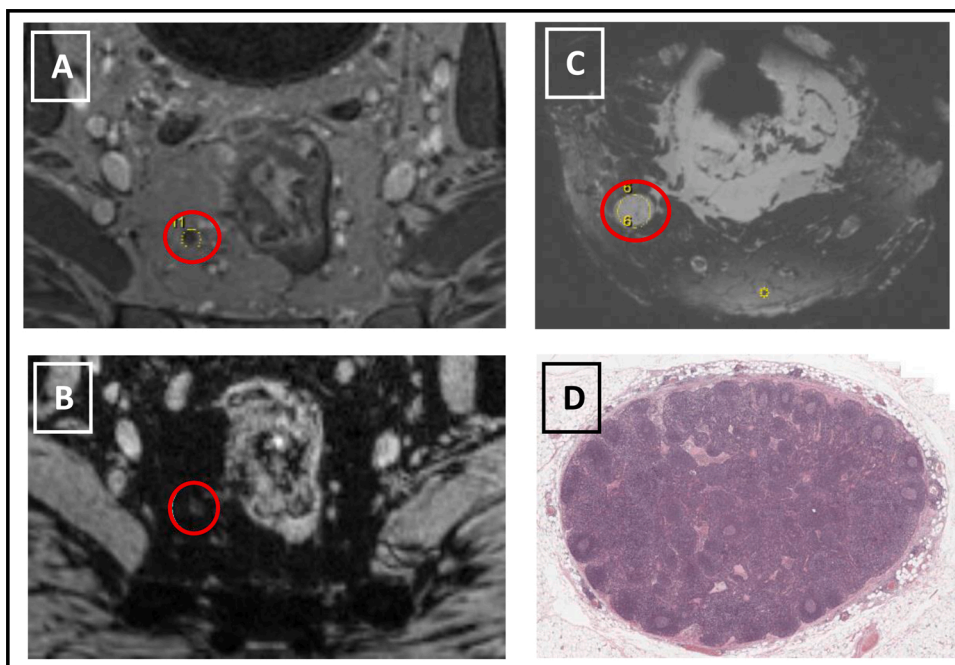
Fig. 5. Node-to-node matching of a negative lymph node (red circle). A lymph node displayed in the transverse plane of the in-phase image of the VIBE-DIXON dataset (A) defined as nodal type 1 by both readers on the T2*-weighted, iron-sensitive image of water content 24-36 h after infusion of Ferumoxtran-10 (B). The lymph node was matched to the water selected pulse sequence *ex-vivo* MRI (C). This node was non-metastatic with a physiological immune response with reactive follicles on histopathology (D).

contained a limited number of matched lymph nodes that contained tumor metastases which might be due to the inclusion of non-locally advanced or LARC treated with nCRT.

To conclude, the current study is the first to present 3-dimensional 3 T USPIO-enhanced MRI in rectal cancer patients correlated to histopathology. Lymph nodes with high signal intensity on *in-vivo* MRI were either benign with high immunologic activity or contained metastases. There are challenges to overcome regarding to improve node-to-node matching from clinical MRI to pathology. Further prospective studies are needed to provide more insight into the function and behavior of lymph nodes in rectal cancer and improvements are to be made to

correlate smaller lymph nodes to histopathological findings.

CRediT authorship contribution statement

Rutger Stijns: Conceptualization, Methodology, Formal analysis, Investigation, Data original, Writing draft, Visualization, Supervision, Project administration. **Bart Philips:** Conceptualization, Methodology, Software, Investigation, Data curation, Writing review. **Iris Nagtegaal:** Investigation, Data curation, Writing review. **Fatih Polat:** Investigation, Data curation, Writing review. **Johannes de Wilt:** Validation, Investigation, Data curation, Writing review. **Carla Wauters:** Investigation,
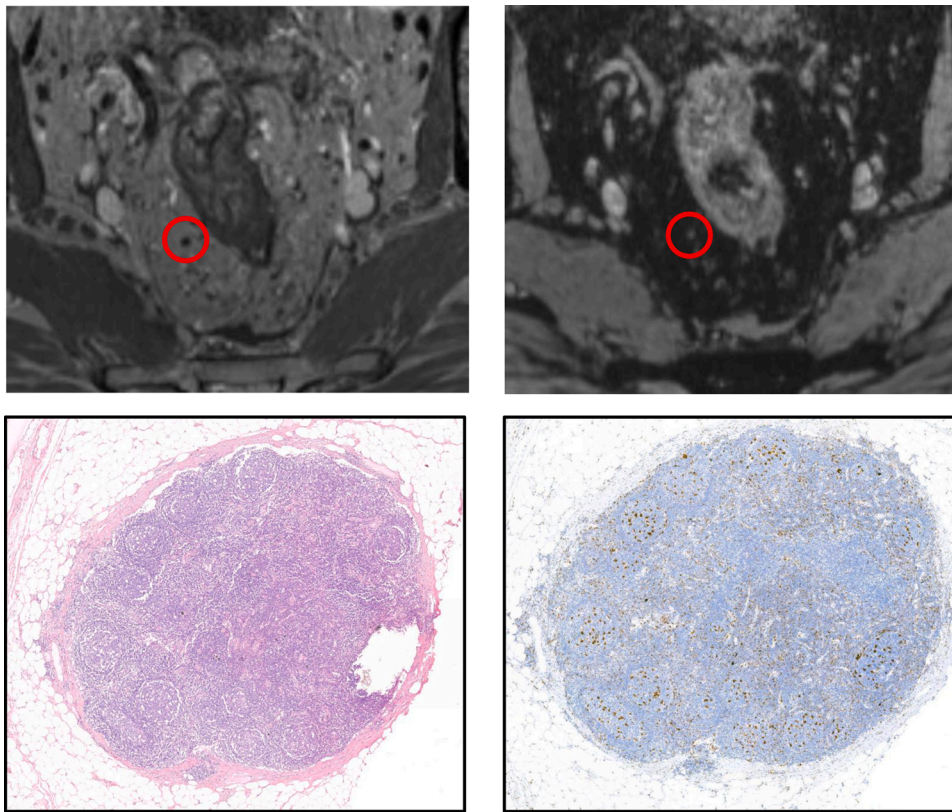
Fig. 6. Representation of a lymph node recognized on VIBE-DIXON MRI sequence (top left) and described as a type 1 node on the T2*-weighted MRI 24-36 h after infusion of Ferumoxtran-10 (top right). Immunohistochemistry showed a non-metastatic lymph node. H&E staining (bottom left) and CD68 immunostaining (bottom right) showed a normal distribution of macrophages throughout the lymph node and throughout the reactive follicles. Macrophages are visualized in the bottom right figure by CD68 uptake resulting in brown deposits within the lymph node.

Data curation, Writing review. **Patrik Zamecnik:** Investigation, Data curation, Writing review. **Jurgen Fütterer:** Investigation, Data curation, Writing review. **Tom Scheenen:** Conceptualization, Methodology, Validation, Investigation, Resources, Writing review, Supervision, Project administration

Declaration of Competing Interest

The conflict of interest for co-author Patrik Zamecnik is the following: dr Zamecnik is a Scientific Advisor to SPL Medical B.V and has options in SPL Medical B.V.

For all other authors or author's institutions there are no conflicts of interest.

Appendix A. Supplementary data

Supplementary material related to this article can be found, in the online version, at doi:https://doi.org/10.1016/j.ejrad.2021.109636.

References

[1] N.P.M. Brouwer, A. Bos, V. Lemmens, P.J. Tanis, N. Hugen, I.D. Nagtegaal, J.H. W. de Wilt, R.H.A. Verhoeven, An overview of 25 years of incidence, treatment and outcome of colorectal cancer patients, Int. J. Cancer 143 (11) (2018) 2758–2766.

[2] R.G.H. Beets-Tan, D.M.J. Lambregts, M. Maas, S. Bipat, B. Barbaro, L. Curvo-Semedo, H.M. Fenlon, M.J. Gollub, S. Gourtsoyianni, S. Halligan, C. Hoeffel, S. H. Kim, A. Laghi, A. Maier, S.R. Rafaelsen, J. Stoker, S.A. Taylor, M.R. Torkzad, L. Blomqvist, Magnetic resonance imaging for clinical management of rectal cancer: updated recommendations from the 2016 European Society of Gastrointestinal and Abdominal Radiology (ESGAR) consensus meeting, Eur. Radiol. (2017).

[3] M.A. Elferink, V. Siesling, V.E. Lemmens, O. Visser, H.J. Rutten, J.H. van Krieken, R.A. Tollenaar, J.A. Langendijk, Variation in lymph node evaluation in rectal cancer: a Dutch nationwide population-based study, Ann. Surg. Oncol. 18 (2) (2011) 386–395.

[4] N.P.M. Brouwer, R.C.H. Stijns, V. Lemmens, I.D. Nagtegaal, R.G.H. Beets-Tan, J. J. Futterer, P.J. Tanis, R.H.A. Verhoeven, J.H.W. de Wilt, Clinical lymph node staging in colorectal cancer; a flip of the coin? Eur. J. Surg. Oncol. 44 (8) (2018) 1241–1246.

[5] M. Cerny, V. Dunet, J.O. Prior, D. Hahnloser, A.D. Wagner, R.A. Meuli, S. Schmidt, Initial staging of locally advanced rectal cancer and regional lymph nodes: comparison of diffusion-weighted MRI with 18F-FDG-PET/CT, Clin. Nucl. Med. 41 (4) (2016) 289–295.

[6] F. Doyon, U.I. Attenberger, D.J. Dinter, S.O. Schoenberg, S. Post, P. Kienle, Clinical relevance of morphologic MRI criteria for the assessment of lymph nodes in patients with rectal cancer, Int. J. Colorectal Dis. 30 (11) (2015) 1541–1546.

[7] L.A. Heijnen, D.M. Lambregts, D. Mondal, M.H. Martens, R.G. Riedl, G.L. Beets, R. G. Beets-Tan, Diffusion-weighted MR imaging in primary rectal cancer staging demonstrates but does not characterise lymph nodes, Eur. Radiol. 23 (12) (2013) 3354–3360.

[8] M.M. van Heeswijk, D.M. Lambregts, W.M. Palm, B.M. Hendriks, M. Maas, G. L. Beets, R.G. Beets-Tan, DWI for assessment of rectal cancer nodes after chemoradiotherapy: is the absence of nodes at DWI proof of a negative nodal status? AJR Am. J. Roentgenol. 208 (3) (2017) W79–w84.

[9] H. Zhang, C. Zhang, Z. Zheng, F. Ye, Y. Liu, S. Zou, C. Zhou, Chemical shift effect predicting lymph node status in rectal cancer using high-resolution MR imaging with node-for-node matched histopathological validation, Eur. Radiol. 27 (9) (2017) 3845–3855.

[10] D.M. Koh, C. George, L. Temple, D.J. Collins, P. Toomey, A. Raja, N. Bett, S. Farhat, J.E. Husband, G. Brown, Diagnostic accuracy of nodal enhancement pattern of rectal cancer at MRI enhanced with ultrasmall superparamagnetic iron oxide: findings in pathologically matched mesorectal lymph nodes, AJR Am. J. Roentgenol. 194 (6) (2010) W505–13.

[11] G. Langman, A. Patel, D.M. Bowley, Size and distribution of lymph nodes in rectal cancer resection specimens, Dis. Colon Rectum 58 (4) (2015) 406–414.

[12] C. Wang, Z. Zhou, Z. Wang, Y. Zheng, G. Zhao, Y. Yu, Z. Cheng, D. Chen, W. Liu, Patterns of neoplastic foci and lymph node micrometastasis within the mesorectum, Langenbecks Arch. Surg. 390 (4) (2005) 312–318.

[13] L. Gietelink, M. Wouters, C.A.M. Marijnen, J. van Groningen, N. van Leersum, R.G. H. Beets-Tan, R. Tollenaar, P.J. Tanis, Changes in nationwide use of preoperative radiotherapy for rectal cancer after revision of the national colorectal cancer guideline, Eur. J. Surg. Oncol. 43 (7) (2017) 1297–1303.

[14] A.S. Fortuin, R. Bruggemann, J. van der Linden, I. Panfilov, B. Israel, T. W. Scheenen, J.O. Barentsz, Ultra-small superparamagnetic iron oxides for metastatic lymph node detection: back on the block, Wiley Interdiscip. Rev. Nanomed. Nanobiotechnol. (2017).

[15] R. Weissleder, G. Elizondo, J. Wittenberg, A.S. Lee, L. Josephson, T.J. Brady, Ultrasmall superparamagnetic iron oxide: an intravenous contrast agent for assessing lymph nodes with MR imaging, Radiology 175 (2) (1990) 494–498.

[16] G. Frija, O. Clement, O. Le Guen, C.A. Cuenod, N. Siauve, S. Benderbous, Experimental investigation of the delivery pathway of ultrasmall

superparamagnetic iron oxide to lymph nodes, Acad. Radiol. 3 (Suppl 2) (1996) S299–300.

[17] L. Wu, Y. Cao, C. Liao, J. Huang, F. Gao, Diagnostic performance of USPIO-enhanced MRI for lymph-node metastases in different body regions: a meta-analysis, Eur. J. Radiol. 80 (2) (2011) 582–589.

[18] M.J. Lahaye, G.L. Beets, S.M. Engelen, A.G. Kessels, A.P. de Bruine, H.W. Kwee, J. M. van Engelshoven, C.J. van de Velde, R.G. Beets-Tan, Locally advanced rectal cancer: MR imaging for restaging after neoadjuvant radiation therapy with concomitant chemotherapy. Part II. What are the criteria to predict involved lymph nodes? Radiology 252 (1) (2009) 81–91.

[19] M.J. Lahaye, S.M. Engelen, A.G. Kessels, A.P. de Bruine, M.F. von Meyenfeldt, J. M. van Engelshoven, C.J. van de Velde, G.L. Beets, R.G. Beets-Tan, USPIO-enhanced MR imaging for nodal staging in patients with primary rectal cancer: predictive criteria, Radiology 246 (3) (2008) 804–811.

[20] D.M. Koh, G. Brown, L. Temple, A. Raja, P. Toomey, N. Bett, A.R. Norman, J. E. Husband, Rectal cancer: mesorectal lymph nodes at MR imaging with USPIO versus histopathologic findings–initial observations, Radiology 231 (1) (2004) 91–99.

[21] M.G. Harisinghani, J. Barentsz, P.F. Hahn, W.M. Deserno, S. Tabatabaei, C.H. van de Kaa, J. de la Rosette, R. Weissleder, Noninvasive detection of clinically occult lymph-node metastases in prostate cancer, N. Engl. J. Med. 348 (25) (2003) 2491–2499.

[22] R.A. Heesakkers, J.J. Futterer, A.M. Hovels, H.C. van den Bosch, T.W. Scheenen, Y. L. Hoogeveen, J.O. Barentsz, Prostate cancer evaluated with ferumoxtran-10-enhanced T2*-weighted MR Imaging at 1.5 and 3.0 T: early experience, Radiology 239 (2) (2006) 481–487.

[23] R.J. Heald, R.D. Ryall, Recurrence and survival after total mesorectal excision for rectal cancer, Lancet (London, England) 1 (8496) (1986) 1479–1482.

[24] R. Glynne-Jones, L. Wyrwicz, E. Tiret, G. Brown, C. Rodel, A. Cervantes, D. Arnold, Rectal cancer: ESMO clinical practice guidelines for diagnosis, treatment and follow-up, Ann. Oncol. 29 (Supplement_4) (2018) iv263.

[25] B.W.J. Philips, R.C.H. Stijns, S.H.G. Rietsch, S. Brunheim, J.O. Barentsz, A. S. Fortuin, H.H. Quick, S. Orzada, M.C. Maas, T.W.J. Scheenen, USPIO-enhanced MRI of pelvic lymph nodes at 7-T: preliminary experience, Eur. Radiol. 29 (12) (2019) 6529–6538.

[26] M.G. Harisinghani, M.A. Saksena, P.F. Hahn, B. King, J. Kim, M.T. Torabi, R. Weissleder, Ferumoxtran-10-enhanced MR lymphangiography: does contrast-enhanced imaging alone suffice for accurate lymph node characterization? AJR Am. J. Roentgenol. 186 (1) (2006) 144–148.

[27] R. Stijns, B. Philips, C. Wauters, J. de Wilt, I. Nagtegaal, T. Scheenen, Can ex vivo magnetic resonance imaging of rectal cancer specimens improve the mesorectal lymph node yield for pathological examination? Invest. Radiol. 54 (10) (2019) 645–652.

[28] P. Quirke, T. Palmer, G.G. Hutchins, N.P. West, Histopathological work-up of resection specimens, local excisions and biopsies in colorectal cancer, Dig. Dis. (Basel, Switzerland) 30 (Suppl 2) (2012) 2–8.

[29] S. Salmi, H. Siiskonen, R. Sironen, K. Tyynela-Korhonen, B. Hirschovits-Gerz, M. Valkonen, P. Auvinen, S. Pasonen-Seppanen, The number and localization of CD68+ and CD163+ macrophages in different stages of cutaneous melanoma, Melanoma Res. 29 (3) (2019) 237–247.

[30] M.G. Harisinghani, S. Saini, R. Weissleder, P.F. Hahn, R.K. Yantiss, C. Tempany, B. J. Wood, P.R. Mueller, MR lymphangiography using ultrasmall superparamagnetic iron oxide in patients with primary abdominal and pelvic malignancies: radiographic-pathologic correlation, AJR Am. J. Roentgenol. 172 (5) (1999) 1347–1351.

[31] H.D. Xue, J. Lei, Z. Li, D.T. Wang, W.X. Zhou, W. Dai, Z.Y. Jin, Lymph node image with ultrasmall superparamagnetic iron oxide and comparison with pathological result, Zhongguo Yi Xue Ke Xue Yuan Xue Bao 31 (2) (2009) 139–145.

[32] R.C. Stijns, T.W. Scheenen, J.H. de Wilt, J.J. Futterer, R.G. Beets-Tan, The influence of endorectal filling on rectal cancer staging with MRI, Br. J. Radiol. 91 (1089) (2018), 20180205.

[33] D. Lam, Y. Kaneko, A. Scarlett, B. D'Souza, R. Norris, R. Woods, The effect of Formalin fixation on resection margins in colorectal cancer, Int. J. Surg. Pathol. 27 (7) (2019) 700–705.

[34] K. Kawai, T. Morikawa, The effect of formalin fixation on the size of pelvic sidewall lymph nodes, Int. J. Colorectal Dis. 33 (10) (2018) 1493–1495.